

peer reviewed ORIGINAL ARTICLE

## Fabrication of a tissue characterization phantom from indigenous materials for computed tomography electron density calibration.

KP Claude<sup>1</sup> M.Phil. | SNA Tagoe<sup>2</sup> M.Phil. | C Schandorf<sup>3</sup> PhD | JH Amuasi<sup>4</sup> PhD

<sup>1</sup>Medical Physics Intern, Graduate School of Nuclear and Allied Sciences, University of Ghana, Ghana Atomic Energy Commission Campus, Kwabenya, Ghana.

<sup>2</sup>Senior Medical Physicist/Principal Biomedical Scientist, National Centre for Radiotherapy and Nuclear Medicine, Korle Bu Teaching Hospital, Accra, Ghana.

<sup>3</sup>Professor, Radiation Protection, Lecturer, Graduate School of Nuclear and Allied Sciences, University of Ghana, Ghana Atomic Energy Commission Campus, Kwabenya, Ghana.

<sup>4</sup>Professor, Medical Physics, Lecturer, Graduate School of Nuclear and Allied Sciences, University of Ghana, Ghana Atomic Energy Commission Campus, Kwabenya, Ghana.

### Abstract

**Background:** Patient data for treatment planning are usually acquired from a computed tomography (CT) scanner. The acquired data are then downloaded into the treatment planning system (TPS). CT scanners use CT numbers in Hounsfield units to account for tissue inhomogeneities within the human body which are different from the parameters required by TPS to enable the dose computation algorithm of the TPS account for tissue heterogeneities in the dose computation process. TPS, however, requires radiological parameters such as relative electron densities (compared to that of water) of tissues to account for inhomogeneity corrections in radiation dose calculation. Such information can be entered in the treatment planning computers capable of reading CT images and used to enable accurate corrections for tissue heterogeneities on a pixel-by-pixel basis, if necessary. There is therefore a need to establish the correlation between the CT numbers and the relative electron densities, reDs empirically, by scanning a tissue characterisation phantom with CT scanner whose CT number to reD conversion is been determined.

This paper seeks to outline a procedure that can be use to fabricate tissue characterisation phantom from indigenous materials to minimize cost of purchasing a commercial one.

**Materials and methods:** A tissue characterisation phantom was constructed from 4 millimetre (mm) perspex (PMMA) sheets and 16 pieces of 20 millilitre (ml) plastic laboratory specimen collection containers. The tissue characterisation phantom was composed of two cylindrical phantoms designed to represent (mimic) the body and head of a standard adult human. The laboratory specimen collection containers were inserted into equally spaced holes arranged along rings on the circular surfaces of the phantoms, which were concentric to a central hole on each of the phantoms. This was done to ensure accuracy of the scanner's calibration. The centres of the holes on the rings were separated by 7.85 centimetre (cm) for the body phantom and 4.19 cm for the head phantom. The body phantom had nine holes; the head phantom had seven holes. The phantom assembly was air-tightly sealed but two holes with openings were created on each of the phantoms to facilitate filling of the phantoms with water. The effectiveness of the sealing was ascertained by subjecting the phantom through a pressure test to identify possible places of leakage along the bonded areas; leaking areas were amended. Locally available materials, which are rich in calcium, carbon, hydrogen and/or oxygen, and can simulate tissues found in the human body in terms of radiological properties, were sought. These materials were used to fill the specimen collection containers. The reDs of the materials were determined from CT scanning of the constructed phantoms filled with the materials with two different multi-slice CT scanners from different manufacturers. The reDs were confirmed with those obtained from measured linear attenuation coefficient with cobalt 60 beam for the materials. The constructed tissue characterisation phantom was used to calibrate General Electric (GE) LightSpeed® volume CT (VCT) scanners and the results compared to that of a commercial tissue characterisation phantom.

**Result:** Comparing the two approaches used for the determination of the reDs of the inserted materials of the fabricated tissue characterisation phantom, the reDs agreed with each other within  $\pm 8\%$  (mean of 3.77%; standard deviation of 3.01%). The reDs of the constructed tissue characterisation phantom compared very well with that quoted by the manufacturer of the commercial phantom. The agreement of the reDs is within  $\pm 6.6\%$  (mean of  $\pm 3.27\%$ ; standard deviation of  $\pm 2.67\%$ ).

**Conclusion:** The constructed tissue characterisation phantom compares favourably with the commercial one. In view of this the use of the constructed tissue characterisation phantom in clinical environment is recommendable.

### Keywords

CT scanner, relative electron density, inhomogeneity

### Introduction

Image-based treatment planning has become the standard for external beam radiotherapy. Patient data for treatment planning need to be acquire from a com-

puted tomography (CT) scanner to enable downloading the data into the treatment planning system (TPS). CT scanners use CT numbers (in Hounsfield units) to account for tissue inhomogeneities within

the human body, which are different from the parameters required by TPS to enable the dose computation algorithm of the TPS account for tissue heterogeneities in the dose computation process. Such in-

formation can be entered in the treatment planning computers capable of reading CT images and used to enable accurate corrections for tissue heterogeneities on a pixel-by-pixel basis, if necessary. TPS requires radiological parameters, such as relative electron densities (compared to that of water) or physical densities of tissues, to account for inhomogeneity corrections in radiation dose calculation<sup>[1-6]</sup>. Studies have shown that neglect of tissue inhomogeneity correction in treatment plans, especially in lung areas, can result in radiation dose errors exceeding 30 % of the prescribed dose to a patient<sup>[4, 7]</sup>.

The attenuation of a radiation beam traversing a medium is influenced by the linear attenuation coefficient of the medium. This has a direct link to the physical density and the number of electrons per gram of the medium. For clinical megavoltage beams, where Compton scattering is the predominant interaction, electron density within the interacting medium is found to be directly proportional to the magnitude of the Compton scattering. The radiation dose deposited within the medium is influenced by the Compton scattering process<sup>[8]</sup>.

There is therefore the need to determine the relationship between the CT numbers and densities (especially relative electron densities) in each voxel of the CT images. The CT number to radiological parameter relationship is established empirically by scanning a tissue characterisation phantom with the CT scanner whose CT number to radiological property correlation is been established<sup>[5, 6, 9]</sup>. The correlation must be established for all CT scanners use for the acquisition of patient data for treatment planning. CT numbers have been found to be dependent on the individual CT scanner parameters such as kilovoltage peak (kVp) / filtration and reconstruction algorithm<sup>[9, 10]</sup>. In view of this the tissue characterisation phantoms are normally scanned with scan parameters used for scanning patients based on anatomic site. Some TPS comes with built-in CT numbers to radiological conversions curve or look up tables. However, CT scanners which will be use to acquire patient data for the TPS need to be calibrated. The calibrations of the CT scanners need to be done with a tissue characterisation phantom.

There are several commercially available tissue characterisation phantoms that are designed to represent certain segments of the human body, such as the

head and the abdomen. The phantoms are made from tissue substitute materials and have holes that can accommodate inserts made from materials of known radiological properties.

The aim of this paper is to outline a procedure that can be used to fabricate tissue characterisation phantom from locally available materials to minimize cost of purchasing a commercial one.

### Underpinning theory

Most tissue characterisation phantoms are manufactured from a number of tissue substitute materials. The radiological properties, especially the electron density of the materials, must be known to a high degree of accuracy. The electron density may be obtained from the following procedures.

#### • Computation of electron density from mass density and atomic composition

The electron density,  $\rho_e$  of a material may be computed from its mass density,  $\rho_m$  and its atomic composition according to the formula<sup>[11]</sup>:

$$\rho_e = \rho_m \cdot N_A \cdot \left(\frac{Z}{A}\right) \quad (1)$$

Where

$$\left(\frac{Z}{A}\right) = \sum_i a_i \cdot \left(\frac{Z_i}{A_i}\right) \quad (2)$$

And  $N_A$  is Avogadro's number and  $a_i$  is the fraction weight of a constituent element of the material of atomic number  $Z_i$  and atomic weight  $A_i$ .

#### • Determination of electron density from linear attenuation coefficients

Lack of knowledge of the relative detailed elemental chemical compositions for the various materials which were inserted into the fabricated phantom necessitated the used of other nondestructive meanings to determine the electron density of the materials.

Ideally, for a given material to be able to scatter or attenuate radiation in a similar manner as another material, the two materials must have the same effective atomic number, number of electrons per gram (electron density), and mass density. Since Compton effect is the predominant mode of interaction for megavoltage photon beams usually used for clinical treatment means that the necessary condition for the two materials to be equivalent radiologically for such beams requires the materials to have the same electron density (number of electrons per cubic centimetre)<sup>[11]</sup>. This implies that for

a clinical beam the interaction per unit path length (or linear attenuation coefficient) in a medium is directly proportional to the electron density of the medium through which the clinical beam traverses provided beam hardening and softening effect are minimized<sup>[8, 11]</sup>. Thus,

$$\mu = k \rho_e \quad (3)$$

And

$$\mu_w = k \rho_{e, water} \quad (4)$$

where  $\mu$  and  $\mu_w$  are the linear attenuation coefficients of a material and that of water respectively measured using the same clinical beam energy and irradiation geometry;  $\rho_e$  and  $\rho_{e, water}$  are the electron densities of the material and water respectively; and  $k$  is the proportionality constant.

From equations 3 and 4 it implies;

$$\rho_e = \frac{\mu}{\mu_w} \times \rho_{e, water} \quad (5)$$

From equation 5 determining the linear attenuation coefficients of the chosen materials relative to that of water measured with the same clinical beam and irradiation geometry, the electron densities of the materials can be calculated. The electron density,  $\rho_{e, water}$  of water can easily be computed from equations 1 and 2 or obtained from literature<sup>[11]</sup>.

#### • Determination of electron density from CT numbers

Researchers proposed two formulae that tried to link the relative electron density (compared to that of water), reD, of tissues found in the human body to their corresponding CT numbers based on the nature of the tissue having radiological properties that can be approximated to that of water or bone in terms of Hounsfield unit. For soft water-like tissues with low atomic number (Z), such that the CT number,  $N_{CT}$  of the tissue is less than 100, the relative electron density was found to be<sup>[6, 12]</sup>;

$$\rho_e = 1.0 + (0.001 \times N_{CT}) \quad (6)$$

For bone-like tissues with higher Z values, such that  $N_{CT}$  is greater than 100; the relative electron density estimated from;

$$\rho_e = 1.052 + (0.00048 \times N_{CT}) \quad (7)$$

such that;

$$\rho_e = \frac{\rho_e}{\rho_{e, water}} \quad (8)$$

## Materials and methods

### (i) The construction of the tissue characterisation phantom

Two cylindrical phantoms were fabricated from 4 mm thick perspex sheets and 16 pieces of 20 ml plastic laboratory specimen collection containers (each with a diameter of 2.8 cm) to represent the anatomy of the head and abdomen of an average adult. A portable electric jig-saw was used to saw the circular surfaces of the phantoms from the perspex sheets. The two circular surfaces of the same diameter were aligned and firmly clamp together; holes were drilled through them to hold the plastic laboratory specimen collection containers. The holes were arranged in a concentric ring with radii of 10 cm and 4 cm for the abdomen and head phantoms respectively. A hole central to the circular surfaces was also made for each phantom. The phantom abdomen ring was designed to have eight holes equally spaced around the ring. The head phantom had six holes equally spaced around the ring. The sawn circular surfaces were then separated by a distance of 5.6 cms. The containers were then held in place with super glue<sup>®</sup> adhesive so that spaces around the containers and the sawn circular surfaces were air-tightly sealed. Perspex sheets with a width of 6.4 cm and a length slightly longer than the circumference of the sawn circular surfaces were heated in an oven at 140°C to make them flexible. The heated perspex sheets were then wrapped around the sawn circular surfaces and the plastic laboratory specimen collection containers were assembled. The assembled containers were held in position to cool down to a lower temperature. After cooling down the perspex sheets assumed the circular shapes of the phantoms. The excess length was cut out. The moulded perspex sheets that formed the sides of a respective phantom were glued to the circular perspex sheets with trichloromethane (chloroform) at room temperature. The circular perspex sheets constituted the surfaces of the phantoms. Trichloromethane dissolves perspex, thus when applied to two perspex sheet surfaces this causes the surfaces to stick together after the chloroform has completely evaporated. This process occurs at room temperature. The ends of the moulded perspex sheets were also glued to the other end with the chloroform. Gluing was done in such a way as to

make the phantom under construction air-tight. The effectiveness of the sealing was ascertained by subjecting the phantom to a pressure test to identify possible places of leakage along the bonded areas; leaking areas were amended. Two openings with plastic screwed covers fitted with rubber washers were created on one of the surfaces of each phantom to facilitate the filling of them with water. The phantoms are shown in Figure 1.

### (ii) Selecting tissue substitute materials to fill containers inserted into constructed phantoms

Materials that are readily available locally and have physical densities comparable to those of tissues found in the human body were sought (see Table 1). Materials rich in carbon, calcium, hydrogen and oxygen were the most considered. To avoid streak artefacts during CT scanning of the phantoms meant that materials that are metallic in nature were not considered by the researchers. Such artefacts would have adverse effect on the CT numbers obtained for the materials inserted in the phantoms. The chosen materials with their simulating tissues in terms of physical densities ( $\text{g}/\text{cm}^3$ ) are shown in Table 1.

### (iii) Determination of electron densities of the chosen materials

Knowledge of the detailed chemical element constituents of the various chosen materials together with the equations (1) and (2) can be used to calculate the

electron densities of the materials. Since there is lack of documentation to validate the chemical compositions of the chosen materials in terms of weighted fraction of each element it was therefore essential to use other nondestructive means in the determination of the electron densities.

### (iv) Using linear attenuation coefficient measurements

For the transmission measurements a special graduated water-tight tank (dimensions  $8 \times 8 \times 10 \text{ cm}^3$ ) that could be mounted at the accessory holder on the collimator system of the GWGP80 cobalt-60 teletherapy unit (Nuclear Power Institute of China) was designed and fabricated from 4.0 mm perspex sheets (see Figure 2). The fixed accessory hold distance was 45.0 cm from the source of radiation for the teletherapy machine used for the measurements. The measurements were made in air with 0.125 cc Farmer type ionization chamber (PTW 31002-0393, Freiburg) with its build-up cap on, using source to detector distance (SDD) of 100 cm. Materials in the vicinity of detector that could scatter radiation were removed to minimize the amount of scattered radiation reaching the sensitive volume of the ionization chamber. Measurements were made with  $6 \text{ cm} \times 6 \text{ cm}$  (defined at the isocenter of the teletherapy unit) radiation beam from a GWGP80 cobalt-60 teletherapy unit (Nuclear Power Institute of China) with source-to-axis distance (SAD) of 80 cms. The ionization chamber was connected

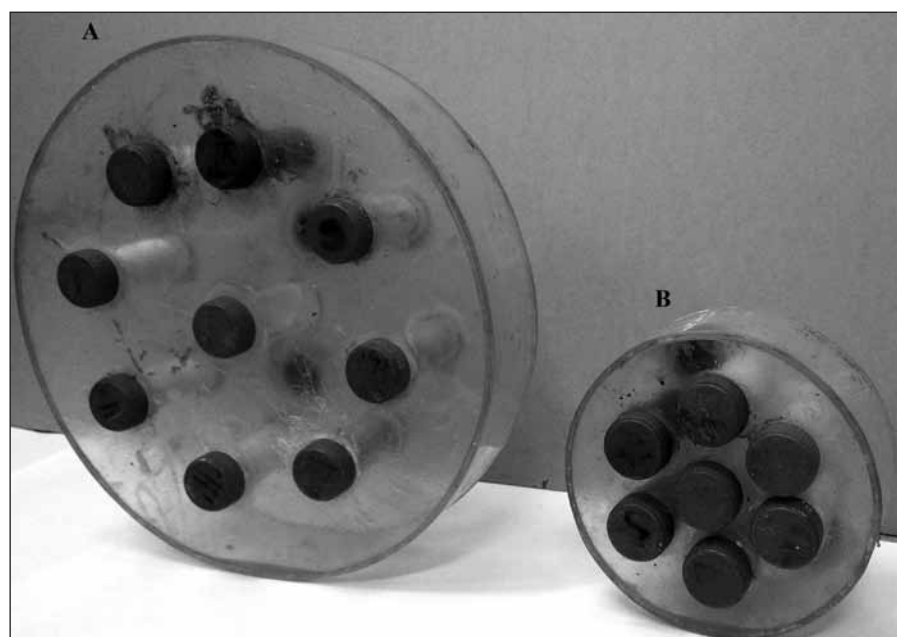


Figure 1: Constructed phantoms not fill with water – (A) phantom representing head and (B) phantom representing abdomen or body.

to a PTW UNIDOS electrometer (serial number; 10002-20204), which was set to measure the intensity of the transmitted radiation through the absorber in terms of charges at 60 seconds interval with a bias voltage of +400 V.

The fabricated tank was filled with water and mounted on the accessory holder of the teletherapy unit. The intensities of the radiation as it travelled through the water were measured for various thicknesses (from 0 to 10 cms at an increment of 2 cms) of water. For each thickness of absorber, successive intensity readings were acquired and the mean reading determined. The mean readings were corrected for influencing factors such as temperature (using a reference of 20°C) and pressure (using a reference of 101.325 Kpa with a humidity of 50%)<sup>[13]</sup>. Using the same irradiation geometry, the measurements were repeated for the chosen materials with which containers inserted into the constructed phantom would be filled. For each set of the measurements the intensity of the radiation beam without the absorber in the tank was also measured. A schematic diagram of the set-up for the measurements of the linear attenuation coefficients of the materials is shown in Figure 3.

Graphs of natural log of measured intensity against thickness absorber were plotted for the materials and water to determine their respective linear attenuation coefficients. The electron densities of the various materials were then calculated from equation (5), from which the relative electron densities,  $reD_{LAC}$ , were computed using equation (8). The correlation between the determined  $reD_{LAC}$  and the measured physical densities is shown in Figure 4.

#### (v) From CT numbers obtained through scanning of the constructed phantoms filled with the materials

The constructed phantoms were filled with water such that there were no air bubbles within the phantoms, and the valves improvised for filling the phantoms were closed. The containers inserted into the phantoms were each filled with a chosen material (see Table 1) whose electron density needed to be determined. The containers were closed with their respective covers to prevent the materials within the containers from spilling. In filling the containers with the chosen materials the researchers ensured that the containers and their contents did

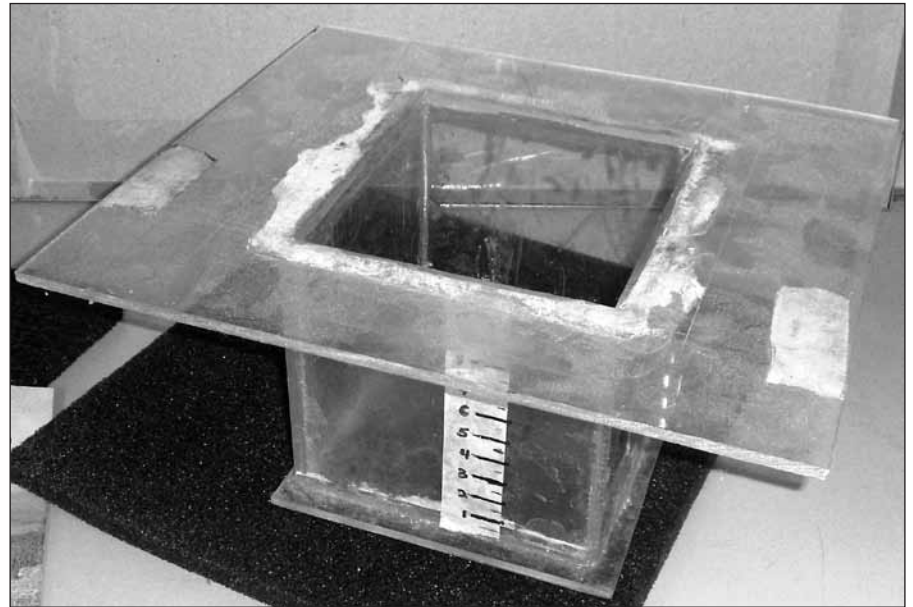


Figure 2: Fabricated tank used for transmission measurements in air.

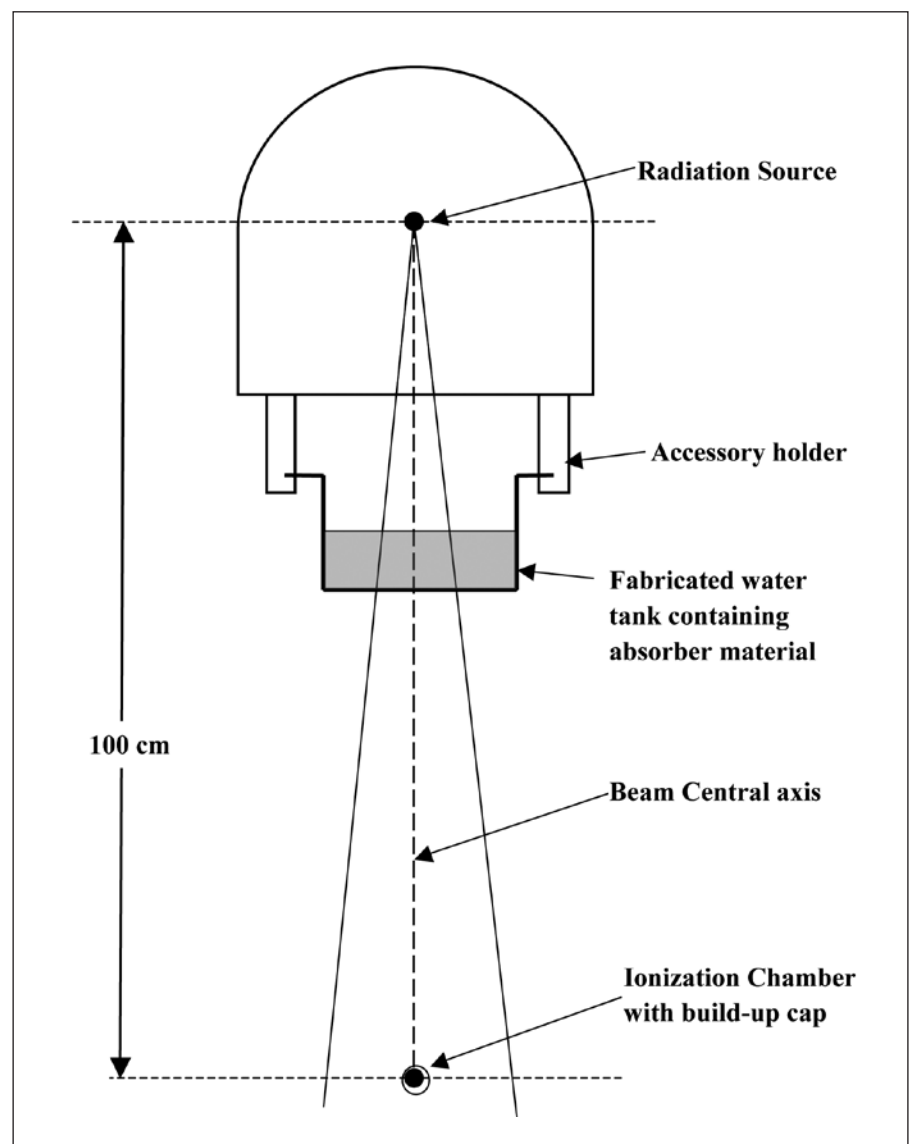


Figure 3: The set up used for determination of linear attenuation coefficient of chosen materials.

not have air-gaps. Samples of the same material were put into the head and body (abdomen) phantoms. The containers in the central part of the phantoms were not filled with any of the materials to ensure the simulation of air within the phantoms.

Since the inserted containers in the phantoms were limited in number, contents of some of the containers were replaced with other materials which had not occupied a container after CT scanning of the phantoms. The phantoms and their contents were once again scanned

after the refilling. The phantoms were scanned with two different multi-slice CT scanners from different manufacturers using slice thickness of 5 mm. During scanning the phantoms were aligned central to the aperture of the CT scanners. The head phantom was scanned with parameters of 80 kVp and a tube current ranging from 250 to 300 mAs. The abdomen phantom was scanned with parameters of 120 kVp and a tube current ranging from 350 to 400 mAs. The CT scanners used for the scans were as follows: LightSpeed VCT scanner (64 slices) manufactured by General Electric (GE) Medical Systems; and ECLOS CT scanner (16 slices) from Hitachi Medical Corporation. Both CT scanners have a bore size of 70 cm and a 50 cm field of view.

After scanning the phantom, a 1.0 cm<sup>2</sup> circular region of interest (ROI) was used to measure the CT numbers of the insert materials. The measurements were done such that the ROI was central to the insert whose CT number was been determined. The mean CT number per inserted material was determined regardless of scan protocol and CT scanner used. From equations (6) and (7), the relative electron densities,  $reD_{CT}$ , of the various inserted materials were computed.

**Checking efficacy of the constructed tissue characterisation phantom**

The relative electron densities obtained from the mean CT numbers for the various insert materials were compared against those obtained from the linear attenuation coefficients to determine whether the discrepancies between the two were not more than 8 %<sup>[6]</sup>. The mean CT numbers with their corresponding relative electron densities of the inserted materials obtained from the CT numbers were used to create a CT number to  $reD$  conversion curve for a Prowess Panther™ version 4.6 TPS (Prowess Systems, Chico, CA, USA). The CT numbers used were those obtained with the LightSpeed VCT scanner. A commercial tissue characterisation phantom 062 M, (CIRS Inc., USA) was borrowed from another oncology centre and scanned with the LightSpeed VCT scanner which was used to scan the constructed tissue characterisation phantom. The phantom scan data obtained were downloaded into the Prowess Panther TPS and the TPS used to determine the  $reDs$  of the various inserts of the commercial tissue characterisation phantom. The  $reDs$  obtained from the TPS

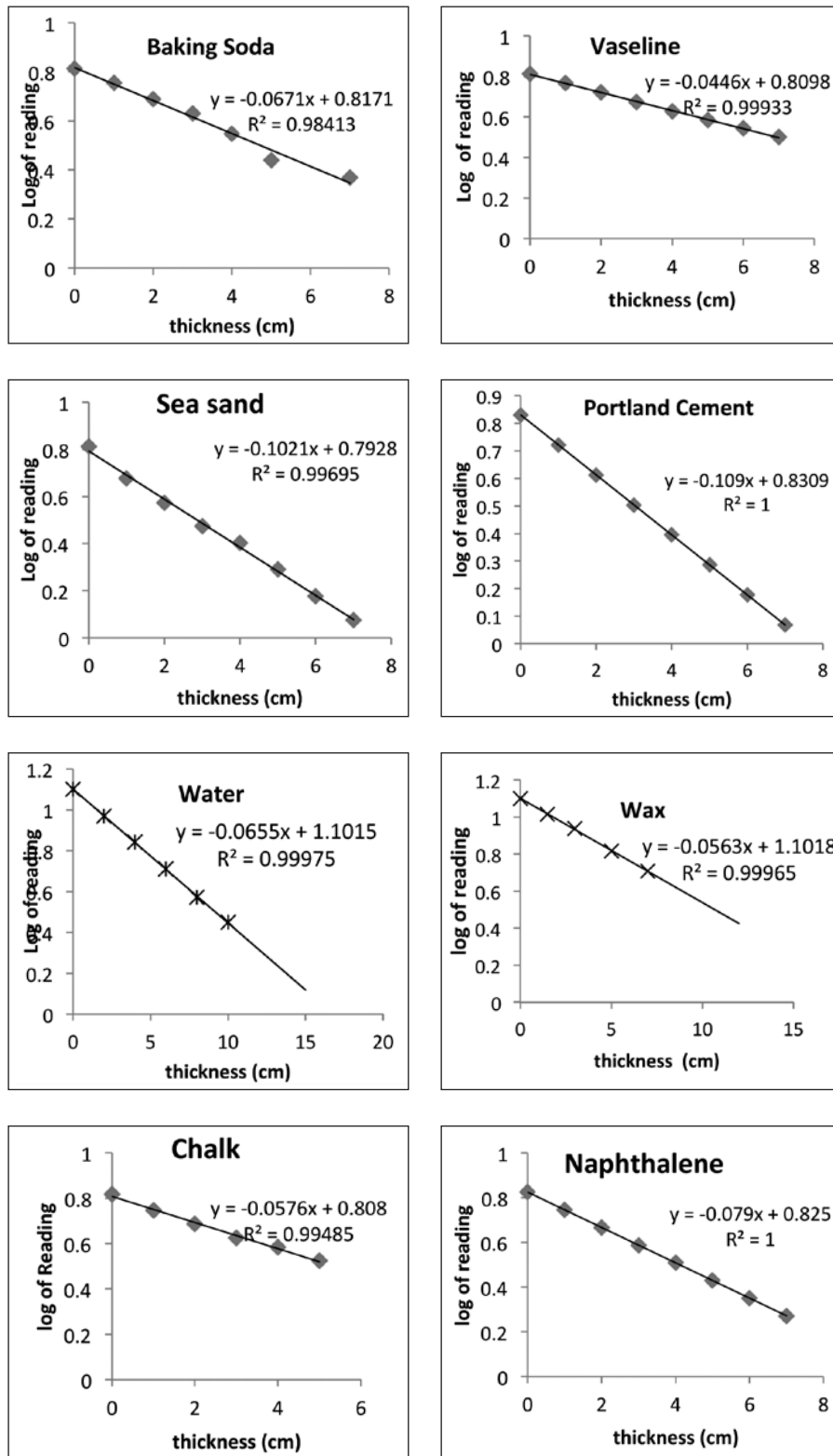


Figure 4: Natural log of detector reading as a function of thickness of inserted materials used for the determination of the linear attenuation coefficients of the selected materials.

were compared to that provided by the manufacturer of the commercial tissue characterisation phantom.

**Results**

The determined relative electron densities of the inserted material of the fabricated phantom are depicted in Figure 4 as a function of the measured physical densities of the materials for both methods used in the determination of the relative electron densities; using the same axes for the plot of the curves. The equations of the correlation for the two methods are displaced on the curves with their respective regression ( $R^2$ ). In Figure 5 the correlations between the transmission readings measured with the ionization chamber and thicknesses of the various materials, which were inserted into the fabricated tissue characterisation phantom, are depicted. The correlation equation for each material from which the linear attenuation coefficient of the specific material was determined is displaced on each curve for the various materials, as well as the regression ( $R^2$ ) for the curve. Figure 6 shows the axial CT images of the constructed tissue characterisation phantom. Image A is that of the phantom designed to represent the body and image B is designed to represent the anatomy of an average adult's head.

Table 1 provides a list of materials which were inserted into the phantom during the CT scanning process. Measured physical densities of the various selected materials are also listed together with the corresponding tissues whose

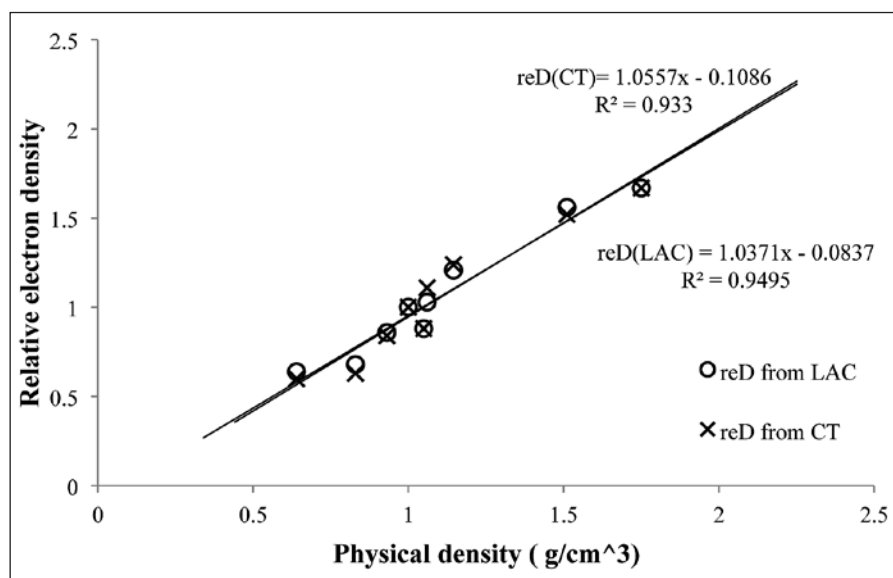


Figure 5: Relative electron densities determined from linear attenuation coefficient (LAC) and that from CT scanning of fabricated phantom as a function of measured physical densities of inserted materials.

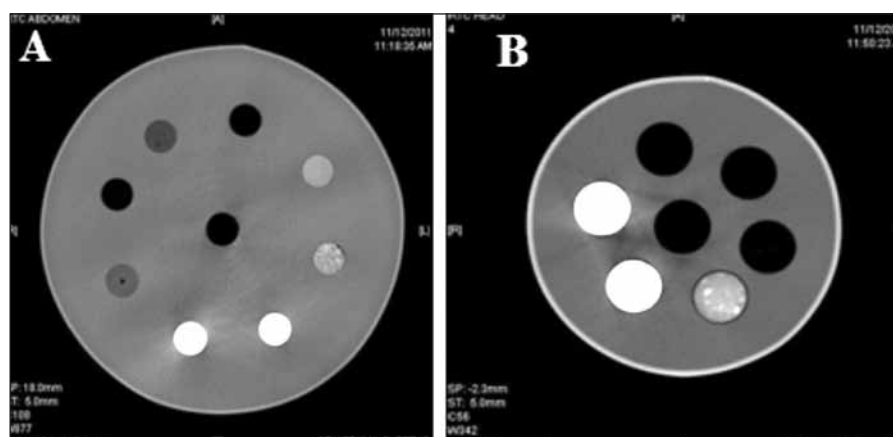


Figure 6: Axial CT images of the constructed CT electron density phantoms. (A) abdomen or body (B) Head.

**Table 1:** Selected materials with their corresponding measured physical densities and simulating tissues.

Materials	Constituent elements	Physical density (g/cm <sup>3</sup> )	Equivalent tissues in the body
Paraffin wax	Hydrogen; Carbon	0.93	Adipose
Water	Hydrogen; Oxygen	1.00	Breast (50% Gland / 50% Adipose)
Powdered naphthalene	Hydrogen; Carbon	1.145	Solid trabecular bone (200 mg/cc HA)
Powdered hardwood charcoal	Carbon	0.64	Lung (exhale)
100% pure petroleum jelly (Vaseline)	Mixture of hydrocarbons	0.83	Brain matter
Powdered chalk	Calcium; Carbon; Oxygen	1.05	Muscle
Sodium bicarbonate (baking soda)	Sodium; Carbon; Oxygen	1.06	Liver
Silicon dioxide (sea sand)	Silicon; Oxygen	1.51	Solid dense bone (800 mg/cc HA)
Portland cement	Calcium; Silicon; Magnesium; Aluminum; Oxygen	1.75	Compact bone (1250 mg/cc HA)

**Table 2:** Radiological properties of selected materials.

Materials	Linear attenuation coefficient $\mu(\text{cm}^{-1})$	Electron density $\rho_e = \mu / \mu_{\text{water}} \times 3.34 \times 10^{23}$ per gram	$reD_{LAC}$ $\rho'_e = \frac{\rho_e}{\rho_{e,\text{water}}}$
Water	0.0655	3.340	1.00
Silicon dioxide (sea sand)	0.1021	5.2063	1.56
Paraffin wax	0.0563	2.8709	0.86
Sodium bicarbonate (baking soda)	0.0671	3.4216	1.03
Portland cement	0.109	5.5582	1.67
100% pure petroleum jelly (Vaseline)	0.0446	2.2743	0.68
Powdered hardwood charcoal	0.0416	2.1213	0.64
Powdered Naphthalene	0.079	4.0284	1.21
Powdered Chalk	0.0576	2.9372	0.88

**Table 3:** Measured CT numbers and reDs calculated from CT numbers for materials inserted into phantoms.

Materials	CT number (HU)			reD <sub>CT</sub> calculated from Mean HU
	LightSpeed VCT	ECLOS	Mean	
Water	0.50	0.47	0.48	1.00
Sea sand	986.20	958.94	972.57	1.52
Chalk	-129.33	-105.74	-117.53	0.88
Baking soda	108.93	129.54	119.23	1.11
Portland cement	1351.54	1230.59	1291.07	1.67
Vaseline	-368.31	-365.63	-366.97	0.63
Charcoal	-410.52	-395.16	-402.84	0.60
Naphthalene	499.49	272.67	386.08	1.24
Wax	-166.04	-160.96	-163.50	0.84
Air	-990.64	-962.95	-976.79	0.02

**Table 4:** Discrepancies between reDs obtained from the two procedures.

Materials	Differences between reDs $reD_{LAC} - reD_{CT}$	Percentage difference (%) $(\frac{reD_{LAC} - reD_{CT}}{reD_{CT}}) \times 100\%$
Water	0	0.00
Sea sand	0.04	2.63
Wax	0.02	2.38
Baking soda	-0.08	-7.21
Portland cement	0	0.00
Vaseline	0.05	7.94
Charcoal	0.04	6.67
Naphthalene	-0.03	-2.42
Chalk	0	0.00

physical properties are been simulated by the selected materials. The chemical elemental constituents of the various materials are listed in Table 1. The radiological properties, linear attenuation coefficients and electron densities, of the various inserted materials in the constructed tissue characterisation phantom are numerated in Table 2. The electron densities as well as the *reDs* were computed from the measured linear attenuation coefficients using equations (5) and (8) respectively. The measured mean CT numbers obtained for the various materials per CT scanner and the mean CT numbers for the two CT scanners per material are listed in Table 3. The calculated relative electron densities from the mean CT numbers for the two CT scanners per material, *reD<sub>CT</sub>*, computed from equations (6) and (7) are also listed in Table 3. The discrepancies in *reD* values obtained using the two procedures are listed in Table 4. In Table 5 the *reD* values of inserts, determined with the TPS for the commercial tissue characterisation phantom that was scanned with the LightSpeed VCT scanner and phantom data downloaded into the TPS, are compared to *reD* values provided by manufacturer of the commercial tissue characterisation phantom. Deviations in the determined *reD* with TPS are expressed as percentage errors of the quoted *reD* values by the manufacturer of the commercial tissue characterisation phantom.

## Discussion

Ideally, the *reDs* determined using the linear attenuation coefficients of the inserted materials should have been the most suitable choice to use in establishing the CT number to *reD* conversion curve for the TPS. This is attested by the high degree of correlation, namely  $R^2 = 0.9495$  observed between the physical densities of the inserted materials of the fabricated phantom and their corresponding *reDs* determined from linear attenuation measurements compared to that of CT having regression of  $R^2 = 0.933$ . The relatively low correlation recorded for the *reDs* determined with CT scanning of the fabricated tissue characterisation phantom with physical densities may be attributed to the effects of beam hardening<sup>[14, 15]</sup>. However, since most of the inserted materials were in a powdered form, there were problems with compactness of the materials when placed in the tank used for the transmission measurements

Table 5: reD comparison of tissue characterization phantoms.

Insert description	reD quoted by manufacturer	reD determined with TPS	Error in reD from that quoted	Percentage error in reD
Dense bone	1.456	1.550	0.0943	6.48
Breast	0.976	0.979	0.0033	0.34
Lung (inhale)	0.190	0.180	-0.0100	-5.26
Muscle	1.043	1.070	0.0270	2.59
Bone (200 mg/cc HA)	1.117	1.179	0.0617	5.52
Liver	1.052	1.069	0.0173	1.65
Adipose	0.949	0.947	-0.0023	-0.25
H <sub>2</sub> O	1.000	1.008	0.0077	0.77
Lung (exhale)	0.489	0.521	0.0320	6.54

compared to when they were placed in the laboratory specimen collection containers. In placing the materials in their respective laboratory specimen collection containers a high pressure was employed to remove all air-gaps. With reference to this it became imperative to use the *reDs* derived from the CT numbers as the specific *reDs* for inserts of the constructed tissue characterisation phantom. Nevertheless, the *reDs* obtained from the linear attenuation coefficients were used to confirm the *reD* values. Comparing the two approaches used for the determination of the *reDs* indicated that the *reDs* agreed with each other within  $\pm 8\%$ , which translates to an error of less than  $\pm 1\%$  in the prescribed radiation dose to a patient whose treatment plan was done with the TPS and inhomogeneity correction applied<sup>[6]</sup>. The measured linear attenuation coefficients of the inserted materials deviate a little from those found in literature due to the irradiation geometry used in the measurement<sup>[14]</sup>. Since the linear attenuation coefficients were related to that of water measured with the same irradiation geometry, the effects resulting in the deviation will cancel out. Although the constructed tissue characterisation phantom did not consider the effects of position of an insert within the phantom on the CT numbers resulting from beam hardening of the scanner x-ray beam it did compare favourably with the commercial tissue characterisation phantom which considered these effects. The *reDs* of the constructed tissue characterisation phantom compared very well with that of the commercial phantom. The agreement of the *reDs* is within  $\pm 6.6\%$  (mean of  $\pm 3.27\%$ ; standard deviation of  $\pm 2.67\%$ ).

### Conclusion

A tissue characterisation phantom was fabricated from locally available materials rich in calcium, carbon, hydrogen and oxygen. Such materials can simulate tissues found in the human body based on radiological properties. The tissue characterisation phantom was designed to represent the head and body of an average adult. The phantom was constructed to assist with the calibration of CT scanners and will be used for the acquisition of patient data for treatment planning. This will facilitate the CT number to relative electron density conversions required by some treatment planning systems to enable effective correction for tissue heterogeneities on voxel-by-voxel basis in the dose computation within the CT images, reconstructed to form the anatomical segment of the human body. This would also minimize cost of purchasing a commercial tissue characterisation phantom. The constructed tissue characterisation phantom compares favourably with a 062M commercial tissue characterisation phantom. The *reD* values of the constructed tissue characterisation phantom are within  $\pm 6.6\%$  (mean of  $\pm 3.27\%$ ; standard deviation of  $\pm 2.67\%$ ) of those quoted by the manufacture of the commercial phantom. The use of the constructed tissue characterisation phantom in a clinical environment is therefore recommendable.

### References

1. Parker RP, Hobdy PA, Cassell KJ. The direct use of CT numbers in radiotherapy dosage calculations for inhomogeneous media. *Phys. Med. Biol.* 1979; 24:802-809. [iopscience.iop.org/0031-9155/24/4/011](http://iopscience.iop.org/0031-9155/24/4/011)
2. Knoos T, Nilsson M, Ahlgren L. A method of conversion of Hounsfield numbers to

- electron density and prediction of macroscopic pair production cross section. *Radiother Oncology* 1986; 5:337-45. [www.sciencedirect.com/science/article/pii/S0167814086801839](http://www.sciencedirect.com/science/article/pii/S0167814086801839)
3. McCullough EC, Holmes TW. Acceptance testing computerized radiation therapy treatment planning systems: direct utilization of CT data. *Med. Phys.* 1985; 12:237-42. [http://pdfserv.aip.org/MPHYA6/vol\\_12/iss\\_2/237\\_1.pdf](http://pdfserv.aip.org/MPHYA6/vol_12/iss_2/237_1.pdf)
4. Constantinou C, Harrington JC, Deward LA. An electron density calibration for CT-based treatment planning computers. *Med Phys.* 1992; 19:325-8. [online.medphys.org/resource/1/mphya6/v19/i2/p325\\_s1](http://online.medphys.org/resource/1/mphya6/v19/i2/p325_s1)
5. Schneider U, Pedroni E, Lomax A. The calibration phantom for CT based treatment planning computers. *Phys Med Biol.* 1996; 41:111-124. [http://scipp.ucsc.edu/outreach/hartmut/radiobio/pCT\\_lit/Schneider%20U%201996.pdf](http://scipp.ucsc.edu/outreach/hartmut/radiobio/pCT_lit/Schneider%20U%201996.pdf)
6. Thomas SJ. Relative electron density calibration of CT scanners for radiotherapy. *BJR.* 1999; 72:781-786. [bjr.birjournals.org/content/72/860/781.full.pdf](http://bjr.birjournals.org/content/72/860/781.full.pdf)
7. Mackie T.R, El-Khatib E, Battista J, et al. Lung dose corrections for 6 and 15 MV X-rays. *Med Phys.* 1985; 12:327. [pdfserv.aip.org/MPHYA6/vol\\_12/iss\\_3/327\\_1.pdf](http://pdfserv.aip.org/MPHYA6/vol_12/iss_3/327_1.pdf)
8. Watanabe Y. Derivation of linear attenuation coefficients from CT numbers for low-energy photons. *Phys Med Biol.* 1999; 44(9):2201-11 <http://iopscience.iop.org/0031-9155/44/9/308>
9. Cheng B, Saw CB, Alphonse L, et al. Determination of CT-to-density conversion relationship for image-based treatment planning systems. *Med Dosim.* 2005; 30:145-148 [bscw.rediris.es/pub/bscw.cgi/d864947/Determination\\_of\\_CT-to-density\\_conversion\\_relationship\\_for\\_image-based\\_treatment\\_planning\\_systems.pdf](http://bscw.rediris.es/pub/bscw.cgi/d864947/Determination_of_CT-to-density_conversion_relationship_for_image-based_treatment_planning_systems.pdf)

10. Ebert MA, Lambert J, Greer PB. CT-ED conversion on GE LightSpeed RT scanner: influence of scanner settings. *Australas Phys Eng Sci Med.* 2008; 31(2):154-9 <http://www.springerlink.com/index/y340621144816167.pdf>
11. Khan FM. *Physics of radiation therapy.* 2<sup>nd</sup> ed. Baltimore: Lippincott Williams & Wilkins. 2001:160-161.
12. Battista JJ, Rider WD, van Dyke J. Computed tomography for radiotherapy planning. *Int J Rad. Oncol Biol Phys.* 1980; 6:99-107 <http://www.sciencedirect.com/science/article/pii/0360301680902114>
13. International Atomic Energy Agency. Absorbed dose determination in external beam radiotherapy: an international code of practice for dosimetry based on standards of absorbed dose to water, IAEA TECH No. 398 Vienna, Austria: IAEA, 2000: 49 [www-pub.iaea.org/mtcd/publications/pdf/trs398\\_scr.pdf](http://www-pub.iaea.org/mtcd/publications/pdf/trs398_scr.pdf)
14. Weidenmaier W, Christ G. The effect of beam hardening on CT values. *Rofo.* 1985; 143(6):697-701 <http://www.ncbi.nlm.nih.gov/pubmed/3001864>
15. Schultz E, Lackner K. Effects of beam weakening and beam hardening on the measured CT values. *Computertomographie.* 1981; 1(2):83-8. <http://www.ncbi.nlm.nih.gov/pubmed/7187286>
16. Chantler CT, Olsen K, Dragoset RA, Chang J, Kishore AR, Kotochigova SA, Zucker, DS. "X-Ray form factor, attenuation and scattering tables (version 2.1)". National Institute of Standards and Technology (NIST), 1996. <http://physics.nist.gov/PhysRefData/XrayMassCoef/tab4.html>